Chapter 2

The Shape and Figure Rotation of NGC 2915's Dark Halo

Abstract

NGC 2915 is a blue compact dwarf galaxy with a very extended H I disk. This disk shows a short central bar and extended spiral arms, both reaching far beyond the optical component. We use Tremaine & Weinberg's (1984) method to measure the pattern speed of the bar and spiral arms from H I radio synthesis data. Our measurements yield a pattern speed of $\Omega_p = 0.21 \pm 0.06$ km s^{-1} arcsec^{-1} (8.0 ± 2.4 km s^{-1} kpc^{-1} for $D = 5.3$ Mpc), which is inconsistent with the generic property of self-consistent barred disks, that corotation lies just outside the end of the bar. Our adopted bar semi-length $r_b \approx 180''$ puts corotation at more than 1.7 r_b. Because NGC 2915 is isolated, gravitational interactions cannot account for the structure observed in the H I disk. We also demonstrate that the low surface density in the disk and the location of the pseudo-rings make it unlikely that swing amplification (Toomre 1981) or bar-driven spiral arms can explain the bar and spiral pattern. Based on the similarity of the dark matter and H I surface density profiles, we discuss the possibility of dark matter distributed in a disk and following closely the H I distribution. This disk then becomes gravitationally unstable and can naturally form a bar and spiral pattern. However, this explanation is difficult to reconcile with some of the properties of NGC 2915.

Finally, we consider the effect of a massive and extended triaxial dark matter halo with a rotating figure. The existence of such halos is supported by CDM simulations displaying strongly triaxial dark halos with slow figure rotation. The observed structure of the H I disk can then arise through forcing by the rotating triaxial figure. We associate the measured H I pattern speed in NGC 2915 with the rotation of the figure of its dark halo.

2.1 Introduction

About 30% of spiral galaxies are strongly barred. This fraction is roughly doubled if weaker bar-like asymmetries are included. Barred spirals are thus the norm rather than the exception among disk galaxies. The study of barred spiral galaxies is therefore an important field of galactic structure and dynamics, and we refer the reader to the review by Sellwood & Wilkinson (1993).

The form of the potential and the bar pattern speed (Ω_p) are the most important quantities determining the structure and dynamics of a barred spiral disk. N-body simulations of bars (e.g. Sellwood 1981; Combes & Sanders 1981) and analytical calculations (e.g. Contopoulos 1980; Contopoulos & Grosbøl 1989) have shown that for bars to be self-consistent, their pattern speed should be such that corotation occurs just outside the end of the bar. However, measuring the pattern speed of bars is not an easy task and most methods are rather indirect (see, e.g., Schwarz 1981, 1984; Athanassoula 1992b). The method proposed by Tremaine & Weinberg (1984) is the only direct method, relying on little theory and observables alone. However, because of the assumptions it makes, the method is rarely applicable to real galaxies and has been applied successfully to only one object so far (Kent 1987; Merrifield & Kuijken 1995). In this chapter, we apply the Tremaine & Weinberg (TW) method to the galaxy NGC 2915, a blue compact dwarf (BCD) galaxy with a very extended H I disk (Meurer, Mackie, & Carignan 1994, hereafter MMC94; Meurer et al. 1996, hereafter MCBF96). This disk shows a late barred spiral galaxy morphology extending far beyond the optical component.

While the formation of bars is now fairly well understood, the formation of the spiral patterns seen in many spiral disks remains an open issue. Various mechanisms have been proposed to form and maintain spiral patterns. We will consider the most prominent ones here: gravitational interactions (e.g. Noguchi 1987), swing amplification of spiral density waves (Toomre 1981), and bar-driven spiral arms (e.g. Schwarz 1981). We show that none of these is likely to explain the bar and spiral arms structure observed in the H I disk of NGC 2915.

This problem leads us to consider the background mass distribution in NGC 2915. In order to reproduce their flat rotation curves, disks are commonly believed to be immersed in massive dark halos (e.g. Carignan & Freeman 1985). Although the shape of such halos is often assumed to be spherical, there is little observational information on this subject and other shapes are clearly possible (see, e.g., Trimble 1987 and Carr 1994 for reviews). In the particular case of NGC 2915, we demonstrate that a simple rigid spherical halo is unable to explain the properties of the H I disk. We therefore consider other dark matter distributions, including: 1) dark matter distributed in a thin disk following the H I surface density distribution, and 2) dark matter distributed in an extended triaxial halo with a slowly rotating figure.

In § 2.2, we discuss the TW method to measure the pattern speed of bars and review its past applications. In § 2.3, we describe the properties of NGC 2915 and measure its pattern speed. The issues of self-consistency and multiple pattern speeds are mentioned in § 2.4, and in § 2.5 we discuss the possible formation mechanisms for the bar and spiral pattern. In § 2.6, we consider two particular models for the dark matter distribution in NGC 2915. We conclude briefly in § 2.7.

2.2 Pattern Speed Measurement

2.2.1 Indirect Methods

Some indirect methods have been devised to measure the bar pattern speed Ω_p in barred spiral galaxies, and we discuss two of them here. The first one relies on the theory of resonance ring formation (Schwarz 1981, 1984; see also Ousley, Byrd, & Dalla Piazza 1997). It is possible to identify morphological features in the disk of a barred galaxy, such as rings, with the location of known resonances. Using the circular velocity curve and derived epicyclic frequency, the bar pattern speed can then be inferred (see, e.g., Ryder et al. 1996 for recent applications to NGC 1433 and NGC 6300). We apply this method to NGC 2915 in § 2.5. Secondly, it is possible to construct hydrodynamical models of the gas flow in a galaxy (often to reproduce H I observations because of their full kinematical coverage). The hydrodynamical models depend on several parameters of the potential, including Ω_p, so the best fitting model gives an estimate of the bar pattern speed (see, e.g., Lindblad & Kristen 1996 and Lindblad, Lindblad, & Athanassoula 1996 for recent applications to NGC 1300 and NGC 1365). Sellwood & Wilkinson (1993) review many such barred galaxy studies.

Although these indirect methods yield useful information about pattern speeds, it is clearly preferable to have a direct measurement, without relying on theoretical arguments or comparison with dynamical models. We will pursue these indirect methods only as a consistency check of more direct measurements.

2.2.2 Direct Methods

Tremaine & Weinberg (1984) showed that the pattern speed of a barred disk galaxy can be derived from the observed kinematics of a tracer population if (1) there exists a unique, well-defined disk pattern speed Ω_p, and (2) the luminosity density of the tracer satisfies the continuity equation. With these conditions, the pattern speed is given by

$$\Omega_p \sin i = \frac{\int_{-\infty}^{\infty} h(y)dy \int_{-\infty}^{\infty} \Sigma(x,y)[\bar{v}_{los}(x,y) - v_{sys}]dx}{\int_{-\infty}^{\infty} h(y)dy \int_{-\infty}^{\infty} \Sigma(x,y)xdx}, \tag{2.1}$$

where i is the disk inclination, Σ is the surface brightness distribution of the tracer, $\bar{v}_{los}$ is the mean line-of-sight velocity of the tracer, v_{sys} is the systemic velocity of the galaxy, and (x, y) are Cartesian coordinates on the plane of the sky, with the origin at the center of the galaxy and the x-axis parallel to the line of nodes (i.e. the apparent major axis for an intrinsically round disk). These quantities are all observables. The function $h(y)$ is an arbitrary weighting function (see Tremaine & Weinberg 1984). Although the method was intended to measure bar pattern speeds, it can equally be applied to any strong and fairly open pattern, such as spiral arms.

The continuity assumption is valid for a dust-free old stellar population, but may well break down in a dusty system, or when using gas as a tracer (possibility of ionisation, molecular conversion, optical thickness, etc.). In fact, while Tremaine & Weinberg (1984) succeeded in applying their method to an artificial dataset generated from an N-body simulation, they failed on H I data from the barred spiral galaxy NGC 5383 (Sancisi, Allen, & Sullivan 1979). The method is fairly sensitive to noise because only the non-symmetric (i.e. odd in x) part of Σ contributes to the integrals in equation (2.1).

Kent (1987) applied the TW method to the barred spiral galaxy NGC 936. The stellar component of NGC 936 is ideal for this application because it has a strong bar, high surface brightness, high rotation velocity, and is devoid of dust and star formation. The orientation of the system is also favourable. Kent carefully estimated the sources of error in measuring Ω_p. Unfortunately, the relatively poor quality of the kinematical data (by today's standards) led to inconclusive results. He derived an average pattern speed of $\Omega_p = 8.4 \pm 2.9$ km s^{-1} arcsec^{-1} ($\Omega_p = 104 \pm 36$ km s^{-1} kpc^{-1} for $D = 16.6$ Mpc). With Kormendy's (1984) rotation curve, corrected for non-circular motions, and a deprojected bar length of $52''$, corotation then lies between 0.54 and 1.21 bar semi-lengths. This is marginally consistent with the generic result from orbital calculations and self-consistent models of barred spiral galaxies, that corotation occurs just outside the end of the bar (see, e.g., Sellwood 1981; Teuben & Sanders 1985; Athanassoula 1992b).

Merrifield & Kuijken (1995; see also Kuijken & Merrifield 1996) reapplied the TW method to NGC 936, this time with better data and methods. They did not use equation (2.1) directly, but rather used the equivalent formula

$$\Omega_p \sin i = \frac{\langle \bar{v}_{los} \rangle - v_{sys}}{\langle x \rangle} \quad \text{(for a given } y\text{)}, \tag{2.2}$$

where the brackets represent luminosity-weighted averages along the slit. The advantage of this procedure is that the long-slit data can be co-added along the

Table 2.1: Basic Properties of NGC 2915

Quantity	Value	Reference
Position (J2000)	$\alpha = 9^{\rm h}26^{\rm m}11\overset{\rm s}{.}83$	1
Position (J2000)	$\delta = -76°37'35\overset{''}{.}8$	1
Heliocentric Velocity	$V_\odot = 468 \pm 5$ km s^{-1}	2,3
Distance	$D = 5.3 \pm 1.6$ Mpc	1
Classification	I0/BCD	1
Total Apparent B Magnitude	$m_{B_T} = 13.34$ mag	1
Total Absolute B Magnitude	$M_{B_T} = -15.90$ mag	1
B Disk Scalelength	$\alpha_B^{-1} = 25\overset{''}{.}6$ (660 pc)	1
Corrected B Central Surface Brightness	$B(0)_c = 22.44$ mag arcsec^{-2}	1
B Holmberg Radius ($\mu_{B,0} = 26.6$ mag arcsec^{-2})	$R_{{\rm Ho},B} = 1\overset{'}{.}9$ (2.93 kpc)	1
Total H I Flux	$F_{\rm HI} = 145$ Jy km s^{-1}	2
Total H I Mass	$M_{\rm HI} = 9.58 \times 10^8\ M_\odot$	2
H I Velocity Width	$W_{20} = 170$ km s^{-1}	2
H I Extent ($N_{\rm HI,0} = 5 \times 10^{19}$ cm^{-2})	$R_{\rm HI} = 9\overset{'}{.}7$ (14.9 kpc)	2
Dust Mass	$M_{\rm Dust} = 1.05 \times 10^4\ M_\odot$	3
Total Mass (within $r \approx 600'' = 15.4$ kpc)	$M_{\rm Tot} = 2.7 \times 10^{10}\ M_\odot$	2

References for Table 2.1.

(1) Meurer et al. 1994; (2) Meurer et al. 1996; (3) Schmidt & Boller 1992.

spatial axis to measure $\langle \bar{v}_{los} \rangle$, and along the dispersion axis to measure $\langle x \rangle$, yielding higher signal-to-noise measurements. To obtain an unbiased measure of $\langle \bar{v}_{los} \rangle$, Merrifield & Kuijken (1995) also used a deconvolution algorithm allowing for asymmetric Doppler broadening of the spectral lines. They obtained a well-defined average pattern speed of $\Omega_p = 4.8 \pm 1.1$ km s^{-1} arcsec^{-1} ($\Omega_p = 60 \pm 14$ km s^{-1} kpc^{-1} for $D = 16.6$ Mpc). This value puts corotation at $69 \pm 15''$, or 1.3 ± 0.3 bar radii, in good agreement with theoretical expectations.

2.3 NGC 2915

2.3.1 Background

NGC 2915 is a nearby relatively isolated BCD galaxy. MMC94 carried out optical imaging and spectroscopy of NGC 2915 to study its structure, stellar populations, and star formation history. MCBF96 obtained H I synthesis data to study the neutral hydrogen distribution and kinematics, and to model the overall mass distribution (including dark matter). Table 2.1 summarises the basic properties of NGC 2915.

The photometry of MMC94 shows that NGC 2915 has two distinct stellar populations: (1) an exponential red diffuse population in the outer parts ($r \geq 35'' = 0.90$ kpc), with a scale length $\alpha_B^{-1} = 25\farcs6$ (660 pc), an extrapolated central surface brightness $B(0)_c = 22.44$ mag arcsec^{-2} (corrected for inclination and extinction), and constant color; and (2) a slightly peaked core population ($r < 35''$) with increasingly bluer color toward the center. The diffuse population is similar to dwarf elliptical galaxies, but the core is lumpy, contains a young stellar population, and is the locus of high mass star formation. Spectroscopy in the core shows strong Balmer and Ca II H+K absorption lines, and strong narrow emission lines with ratios typical of high excitation low metallicity H II regions. A velocity difference of 60 km s^{-1} is detected across the inner galaxy. If this gradient is due solely to rotation, it corresponds to a deprojected rotational velocity $V_r = 50 \pm 21$ km s^{-1} at $r = 32''$ (neglecting the effects of the bubbles seen in Hα by Marlowe et al. 1995). The associated mass $M_{\rm Core} = 4.8 \times 10^8$ $M_\odot$ for the optical core, with a mass-to-light ratio $M_{\rm Core}/L_B = 1.3$ $M_\odot/L_{B,\odot}$.

The neutral hydrogen observations of NGC 2915 (MCBF96) reveal an H I distribution very different from the optical. Figure 2.1 shows the naturally weighted total H I intensity map overlaid on an optical image of NGC 2915. The H I distribution is unusually extended, up to 5.1 $D_{{\rm Ho},B}$ (22.7 α_B^{-1}), and it has a striking late-type barred spiral galaxy morphology, with two extended spiral arms starting at the end of a central bar. At higher resolution, the H I bar is resolved into two clouds; its semi-length is about $2\farcm4$ (3.7 kpc), and it corresponds roughly in position, orientation, and size to the optical emission. The H I surface density profile is tabulated in Table 2.2. The total H I mass is $M_{\rm HI} = 9.6 \times 10^8$ $M_\odot$, while the H I mass in the bar is only about $5 - 7.5 \times 10^7$ $M_\odot$. Figure 2.2 shows the MCBF96 naturally weighted H I velocity field of NGC 2915, again overlaid on an optical image. It clearly shows the pattern of a rotating disk (with an oval distortion), and suggests the presence of a warp in the outer parts. MCBF96 derived a rotation curve for NGC 2915 using the standard tilted ring algorithm ROTCUR (Begeman 1989). The position angle varies by about 15° and the inclination by about 10° outside of the barred region (where the effects of the bar and a possible warp are hard to disentangle), supporting the presence of a warp in the outer disk. The H I velocity dispersion outside the barred region is the usual $\sigma_v \approx 8$ km s^{-1}, but increases up to 40 km s^{-1} in the central regions (see Table 2.2), a value comparable to the rotation velocities obtained from ROTCUR. This indicates that pressure support is important in the center. MCBF96 applied an asymmetric drift correction to the rotation curve to produce the "circular velocity curve" needed for mass modelling. The circular velocity is tabulated in Table 2.2. It increases rapidly with radius in the inner parts, reaching 80 km s^{-1} by $r = 150''$ (3.9 kpc); it then stays flat until $r = 400 - 450''$ (10.3–11.6 kpc), and increases again up to $\approx$90 km s^{-1} at the last measured point ($r \approx 600'' = 15.4$ kpc).

MCBF96 constructed three-component mass models to interpret the circular

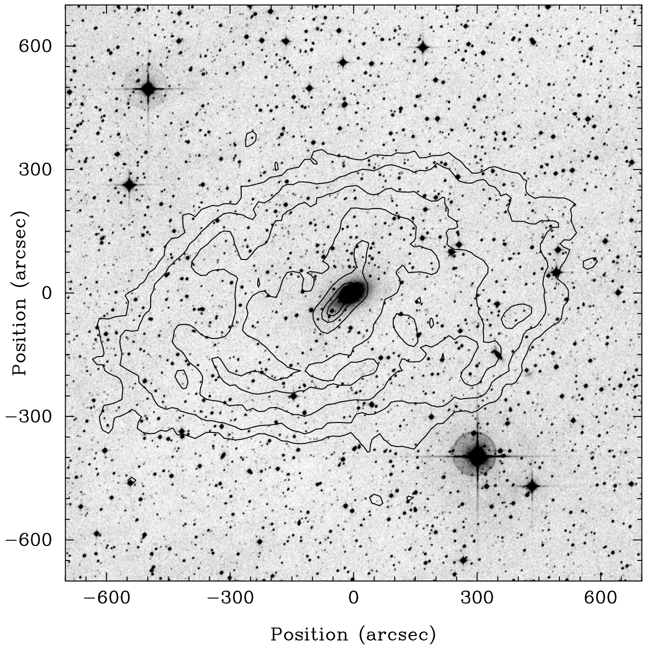

Figure 2.1: Meurer et al. (1996) naturally weighted total H I intensity map, overlaid on an optical image of NGC 2915 (Digitized Sky Survey). The beam is $45'' \times 45''$. Contours levels are 2.5, 7.5, 15, 25, 50, 75, and 90 percent of the peak H I surface brightness of 3.1 Jy beam^{-1} km s^{-1} ($N_{HI} = 1.71 \times 10^{21}$ cm^{-2}).

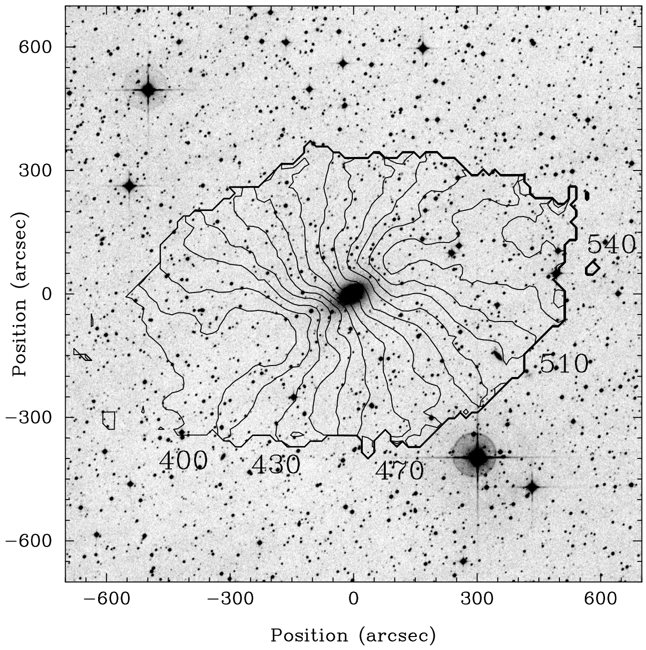

Figure 2.2: Meurer et al. (1996) naturally weighted H I velocity field, overlaid on an optical image of NGC 2915 (Digitized Sky Survey). The beam is $45'' \times 45''$ and the velocity resolution is 6.62 km s^{-1}. Contours are heliocentric velocities separated by 10 km s^{-1}. A few contours are identified on the map.

Table 2.2: Structural and Kinematical Profiles of NGC 2915

r (arcsec)	$\mu_{\rm HI}$ ($M_\odot$ pc^{-2})	μ_B $\left(\frac{B \text{ mag}}{\text{arcsec}^{-2}}\right)$	V_c (km s^{-1})	$\sigma_{V,\rm HI}$ (km s^{-1})	Ω $\left(\frac{\text{km s}^{-1}}{\text{arcsec}^{-1}}\right)$	κ $\left(\frac{\text{km s}^{-1}}{\text{arcsec}^{-1}}\right)$
27.5	8.90	22.55	39.0	33.4	1.42	2.37
52.5	6.35	23.97	53.0	28.8	1.01	1.76
77.5	4.10	25.11	65.0	23.0	0.84	1.44
102.5	3.17	26.26	72.7	20.8	0.71	1.15
127.5	2.53	27.20	76.0	15.6	0.60	0.93
152.5	2.26	28.26	79.2	11.9	0.52	0.81
177.5	2.32	29.32	81.4	10.7	0.46	0.69
202.5	2.36	30.38	82.5	9.9	0.41	0.60
227.5	2.12	31.44	82.8	9.2	0.36	0.48
252.5	1.75	32.50	80.4	10.1	0.32	0.41
277.5	1.49	33.56	80.4	10.1	0.29	0.42
302.5	1.41	34.62	80.9	9.3	0.27	0.38
327.5	1.46	35.68	80.7	8.7	0.25	0.35
352.5	1.43	36.74	80.8	8.3	0.23	0.34
377.5	1.23	37.80	82.0	8.8	0.22	0.32
412.5	1.09	39.28	82.3	8.6	0.20	0.30
457.5	0.89	41.19	83.8	8.1	0.18	0.28
502.5	0.67	43.10	85.5	8.1	0.17	0.28
547.5	0.48	45.01	88.5	8.1	0.16	0.29
592.5	0.32	46.92	93.9	7.7	0.16	0.30

velocity curve. Their models were composed of: (1) a stellar disk, obtained from the B-band surface brightness profile of MMC94 (the mass-to-light ratio M/L_B is a free parameter); (2) an H I disk, based on their observations; and (3) a spherical dark halo (two density distributions were used, both with a central density ρ_0 and core radius r_c as free parameters). All models are dominated by dark matter at all radii. In fact, NGC 2915 is one of the "darkest" disk galaxies known. Its dark matter core is very dense and compact. MCBF96's best fit model[1] has $M/L_B = 1.2\ M_\odot/L_{B,\odot}$, $\rho_0 = 0.10 \pm 0.02\ M_\odot$ pc^{-3}, and $r_c = 1.13 \pm 0.15$ kpc, yielding a total mass $M_T = 2.7 \times 10^{10}\ M_\odot$, $M_T/L_B = 76\ M_\odot/L_{B,\odot}$, and $M_{dark}/M_{luminous} = 19$ within the last measured point.

2.3.2 Pattern Speed

Using the H I data of MCBF96, we now attempt to measure the pattern speed Ω_p of the figure in the disk of NGC 2915. As mentioned in § 2.2.2, the continuity equation imposes a strong constraint on the applicability of the TW method, and

[1]Their model D, with a dark matter density distribution $\rho(r) = \rho_0[1 + (r/r_c)^2]^{-1}$.

gaseous systems are usually thought to be poor candidates for a measurement. NGC 2915 is an unusual galaxy, however, and we argue that the TW method should work for its H I distribution. Firstly, because the stellar component of NGC 2915 is confined to the inner regions of its H I distribution, and the star-forming core to the very center of the H I bar, there is no source of ionising photons over most of the H I disk (except for the weak metagalactic radiation field, and possibly some radiation from the distant core seen by the warped regions). Furthermore, the H I column density is low enough in most of the disk (where the velocity dispersion $\sigma_v \approx 8$ km s^{-1}) that optical thickness problems should not affect the observed H I intensity. Only in the inner parts of the bar, where the optical disk lies, does the column density reach $N_{HI} = 10^{21}$ cm^{-2}, but there the H I velocity dispersion is larger ($\sigma_v \approx$ 20–40 km s^{-1}), so again the optical depth is expected to be low. At this stage, we have no information on possible H I-molecule conversion. However, the low H I column density suggests that this effect is not important. For these reasons, and because the bar and spiral arms pattern is clear and strong, we believe that the TW method applied to the H I distribution and kinematics of NGC 2915 should give a realistic measure of its pattern speed. We note that the orientation of the system is ideal, with the disk at intermediate inclination and the bar oriented about 30° from the major axis of the disk.

We apply the TW method to NGC 2915 using MCBF96's naturally weighted total H I intensity map and velocity field (Fig. 2.1 and 2.2). Additional structural and kinematical parameters describing the galaxy are needed to use the TW method (see § 2.2.2), but these are all provided by the tilted-ring analysis of MCBF96. We use averages of their parameters in the outer disk, outside of the barred region ($r > 150''$): the center of the disk $(x_c, y_c) = (63, 64)$ (in $14''$ pixels), $v_{sys} = 467$ km s^{-1}, and the position angle of the line of nodes PA = 117°. We use equation (2.1) directly, without a weighting function $h(y)$, and for all possible positions y (equivalent to using $h(y) = \delta(y - y_o)$ for each y_o). Because the major axis traces the position of the line of nodes, y is effectively the position of the integration axis along the minor axis of the galaxy. Each offset y provides an independent measurement of the pattern speed. The coordinate system is shown in Figure 2.3, and Figure 2.4a shows the derived pattern speeds as a function of the offset y. The measurements are consistent for most offsets. Only for a few isolated points and for offsets between 0 and $200''$ on the NE side of the galaxy (positive offsets) are the values of $\Omega_p \sin i$ significantly discrepant (recall that the TW method assumes a unique pattern speed for the whole disk, so all offsets should yield similar pattern speeds).

This discrepant region is associated with the northernmost of the two clouds identified by MCBF96, located at the northern end of the bar. Around that region, both the total H I intensity distribution and the velocity field show a

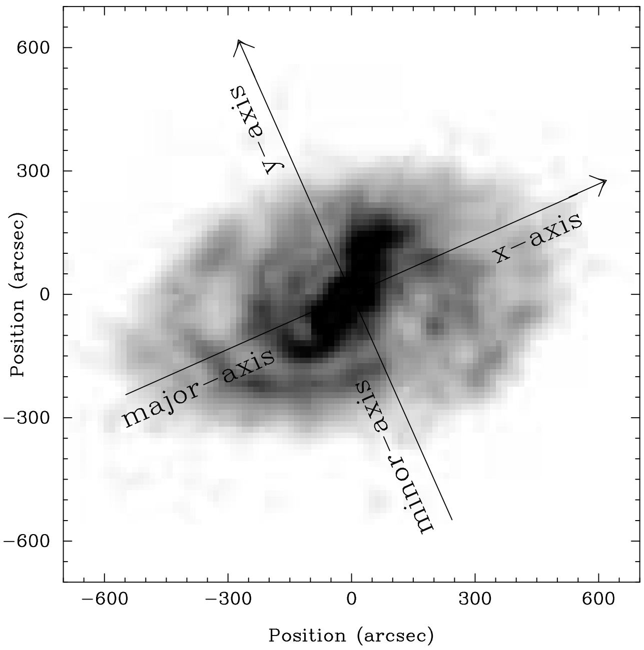

Figure 2.3: Schematised view of the "set-up" required for the Tremaine-Weinberg method calculations (eq. [2.1]), overlaid on a grayscale image of Meurer et al. (1996) naturally weighted total H I intensity map ($45'' \times 45''$ beam).

strong deviation from their large-scale pattern. The discrepancy in the derived pattern speeds therefore probably arises from the fact that the cloud breaks the pattern in the density distribution and/or the velocity field, an effect to which equation (2.1) is very sensitive. Away from this problem region, the pattern speed is well-defined: the entire SW half of the galaxy and the farthest regions in the NE half yield fairly consistent values for $\Omega_p \sin i$. Therefore, we believe that the TW method works for the H I distribution in NGC 2915 and that it gives a reliable estimate of the pattern speed.

In our calculations, we assumed that the parameters required for the TW method measurements were fixed over the whole disk. The center of the disk is well-defined, and only the x-component of the center (x_c) affects the calculations anyway. The systemic velocity is also well constrained, with a small uncertainty of a few km s^{-1}. On the other hand, as shown by the tilted-ring analysis of MCBF96, both the inclination i and position angle PA vary significantly with radius in NGC 2915. A change in inclination affects the pattern speed measurements only through the deprojection. However, a change in position angle materially affects the calculations themselves. We have therefore reapplied the TW method to the H I data of NGC 2915, using a range of values for x_c, v_{sys}, and PA. Although no combination of parameters yields perfectly equal pattern speeds over the whole minor axis, most cases with plausible values show a regular behaviour, with only a restricted range of offsets having very discrepant measurements. A typical good

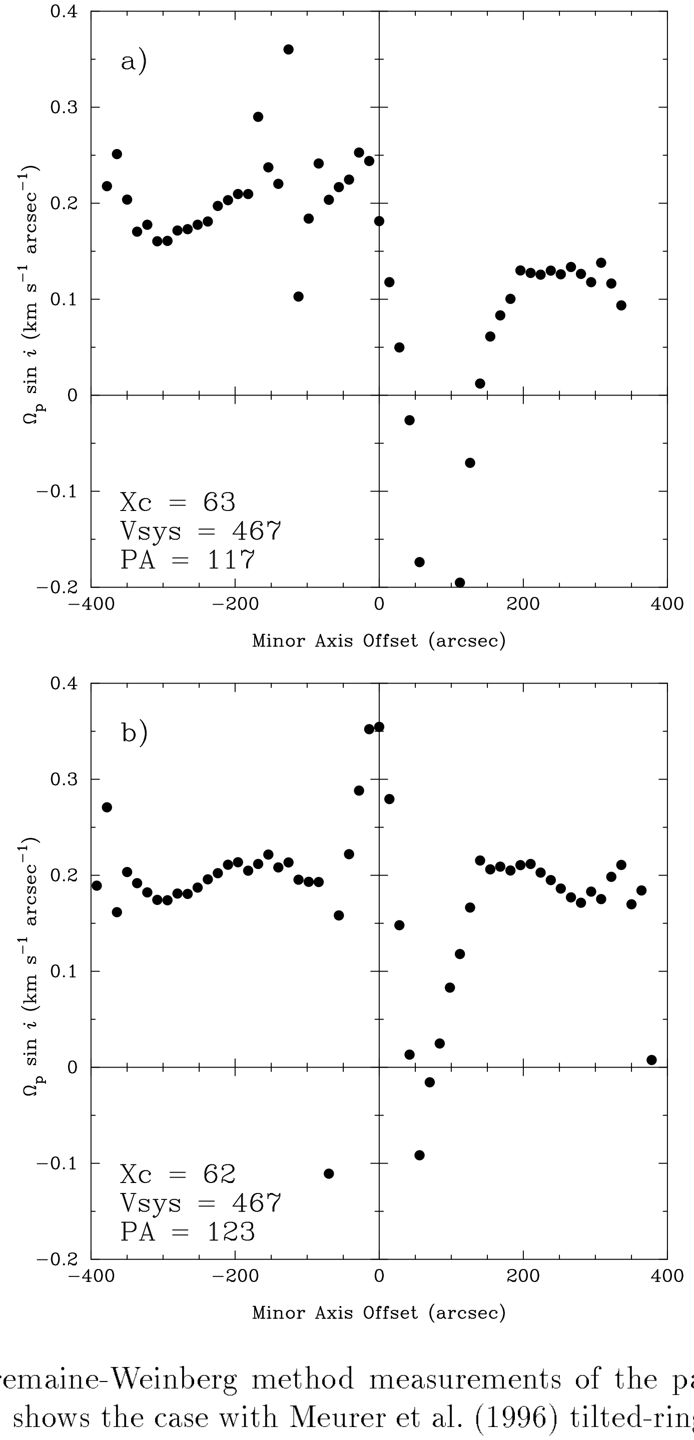

Figure 2.4: Tremaine-Weinberg method measurements of the pattern speed in NGC 2915. (a) shows the case with Meurer et al. (1996) tilted-ring model best fit parameters, while (b) shows a typical good case. Parameters are indicated in the bottom-left corner of each plot.

case is presented in Figure 2.4b.

For all of our estimates, the flat portions of the $\Omega_p \sin i$ "distribution" always lie between $\Omega_p \sin i = 0.12$ km s^{-1} arcsec^{-1} and $\Omega_p \sin i = 0.22$ km s^{-1} arcsec^{-1}. We therefore adopt $\Omega_p \sin i = 0.17 \pm 0.05$ km s^{-1} arcsec^{-1} ($\Omega_p \sin i = 6.6 \pm 1.9$ km s^{-1} kpc^{-1} for $D = 5.3$ Mpc) as our estimate of the pattern speed in NGC 2915. The uncertainty given here represents half the range of measured values for $\Omega_p \sin i$, and is not a standard error estimate. From the outer parts of the disk again, we get an average inclination $i = 56 \pm 3°$. This gives a deprojected pattern speed $\Omega_p = 0.21 \pm 0.06$ km s^{-1} arcsec^{-1} (8.0 ± 2.4 km s^{-1} kpc^{-1}).

The 30% uncertainty in Ω_p is comparable to that achieved by Merrifield & Kuijken (1995) for NGC 936, but is still large given that we are using gas kinematics with the advantage of full two-dimensional spatial coverage. On the other hand, our error estimate (half the range of measured values) is very conservative. As suggested by Tremaine & Weinberg (1984), we tried using odd weighting functions (e.g. $h(y) = \delta(y - y_0) - \delta(y + y_0)$; y_c now affects the calculations directly). Such weighting eliminates the contribution of perturbations with odd azimuthal wavenumbers to the integrals in equation (2.1), and diminishes the effect of centering errors. However, it did not improve our results, as discrepant regions on one side of the minor axis contaminate the combined measurements from both sides. Although we cannot exclude the possibility that the continuity equation is not fully satisfied for the H I in some parts of NGC 2915 (particularly the central regions), we believe that the main sources of error in our measurements are the presence of some short-lived features in the disk (such as the structure seen near the NW cloud) and the warped structure. Tremaine & Weinberg (1984) note that a warp may affect the pattern speed determination, acting as a non-axisymmetric perturbation with zero pattern speed. We repeated the calculations using only the inner barred region of the galaxy, but the results were inconclusive (it is far from clear that the method should work in such a case, as the integrals in eq. [2.1] should extend over the whole system).

2.4 The Nature of the Pattern

2.4.1 Self-Consistent Bars

Many N-body studies show that rotationally supported stellar disks are globally unstable to bisymmetric distortions and quickly form strong bars. This is seen in both two-dimensional (e.g. Sellwood 1981; Athanassoula & Sellwood 1986) and three-dimensional (e.g. Combes & Sanders 1981; Raha et al. 1991) simulations. These instabilities can be identified with the dominant linear modes found in analytical global stability analyses of axisymmetric disks (e.g. Kalnajs 1971, 1977).

The main characteristic of the stellar bars formed in such self-consistent disks is that the bar ends at or just inside its corotation radius (where $\Omega_p = \Omega(r)$).

Orbital calculations in barred disk potentials also support the view that bars end at or just inside corotation (see, e.g., Contopoulos 1980; Athanassoula 1992a; for a review of the orbital structure of barred disks, see Contopoulos & Grosbøl 1989). The argument is that the bar-shaped x_1 orbits, believed to support self-consistent bars, extend close to but not past corotation.

This generic property of self-consistent barred disks does not appear to hold in NGC 2915. The gaseous bar ends well within corotation. We take the ends of the bar to be defined by the regions where the density of the rectangular-shaped central component in the H I distribution drops rapidly; these are also the regions where the spiral arms start. The observed semi-length of the bar is then 145″, with a deprojected value $r_b \approx 180''$. Using our adopted pattern speed, $\Omega_p = 0.21 \pm 0.06$ km s^{-1} arcsec^{-1} (see § 2.3.2), and MCBF96's circular velocity curve (see Table 2.2), corotation occurs at a radius $r_{co} = 390^{+\infty}_{-80}$ arcsec (see Fig. 2.7). Therefore, the ratio of corotation to the bar semi-length is very large, $r_{co}/r_b > 1.7$, and the bar is slowly rotating.

Such a bar is inconsistent with the properties of self-consistent disks and we must conclude that the bar is not due to global bisymmetric unstable modes. It is thus unlikely that the bar and disk are self-gravitating. This is not surprising, considering that the galaxy is completely dominated by dark matter, even in the central regions (MCBF96).

In that regard, we note that dense dark halos have been predicted to slow down bars significantly, as the bar can transfer angular momentum to the outer disk and halo through dynamical friction (see Sellwood 1980; Weinberg 1985; Debattista & Sellwood 1998). These studies used purely stellar models, with a stellar bar, and excluded gaseous processes, some of which may lead to an increase of the bar pattern speed (see, e.g., Kalnajs 1996). They therefore probably overestimate the deceleration rate of the bar, especially in very gaseous disks. Nevertheless, it would be interesting to know how relevant this process might be to the situation observed in NGC 2915.

2.4.2 Bar or Spiral Arms Pattern Speed?

The TW method measures the pattern speed of a disk, taken to be unique. While it was designed to measure the pattern speed of bars, it equally applies to any pattern present in a disk, as long as it is strong enough. It is therefore important to establish the component from which we are measuring the pattern speed. Are we measuring the pattern speed of the bar, the spiral arms, or a common pattern speed for both?

Sellwood & Sparke (1988) suggest that spiral arms in barred spiral galaxies could have a different (lower) pattern speed than the bar. Their work was aimed primarily at explaining the presence of dust lanes on the inner edge of spiral arms in many objects. A lower pattern speed for the spiral would allow the gas to overtake the pattern and therefore lie within its corotation radius in that region, while still retaining the view that bars end at or just inside *their* corotation radius. Sellwood & Sparke (1988) support their suggestion with N-body simulations of barred galaxies showing outer spiral patterns slower than the bar patterns (e.g. Sparke & Sellwood 1987).

Tagger et al. (1987) and Sygnet et al. (1988) develop the idea that the non-linear coupling of (two) modes with different pattern speeds could sustain spiral structure for a long time. For the mechanism to be efficient, resonances of the two patterns must be closely spaced. They observe this effect in many N-body simulations, where the corotation radius of the bar and the inner Lindblad resonance (ILR) of the spiral pattern are very close (this is also the region where the bar ends and the spiral arms begin). The beat wave generated is then axisymmetric and close to its Lindblad resonance and couples non-linearly to the bar and spiral arms.

If we assume that the pattern speed measured here is that of the spiral arms, and that the corotation radius of the bar lies close to the ILR of the spiral pattern, as suggested by Tagger et al. (1987) and Sygnet et al. (1988), we obtain a bar corotation radius $r_{co} < 50''$ (see Fig. 2.7), well inside the bar observed in H I ($r_b \approx 180''$). Such a view would be difficult to defend, considering the body of analytical and numerical work which requires the corotation radius to lie *at least* just outside the bar. This is a strong indication that we are in fact measuring the pattern speed of the bar.

Furthermore, considering the form of equation (2.1), we see that for small minor axis offsets ($y < 90''$), both the central (barred) and external (non-barred) regions of the galaxy contribute to the integrals, while for large offsets ($y > 90''$), the integration axis does not cross the barred region and only the outer parts of the disk contribute to the pattern speed calculations. If the bar and spiral arms had significantly different pattern speeds, we would expect the TW method to fail for small offsets. However, excluding the discrepant points 0–200$''$ on the NE side (which we attribute to a large H I cloud, see § 2.3.2), the pattern speed measurements yield a relatively constant value for all offsets (and for most reasonable combinations of parameters). Considering the relatively small extent of the barred region and the importance of the flux in the outer parts of the disk, it might appear that the spiral arms could dominate the contribution to the integrals in equation (2.1) even for small offsets. This is not so, however: for small offsets, both the barred region and outer parts of the disk contribute significantly to the numerator. It is therefore very likely that a unique pattern speed is being measured. This view is further strengthened by the fact that the spiral arms in NGC 2915 appear to start from the end of the bar (although Sellwood & Sparke 1988 showed that this is not a strong argument).

We therefore adopt the view that the pattern speed which we have measured in § 2.3.2 *is* the unique, common pattern speed of both the bar and the spiral arms, although we cannot entirely exclude yet the possibility that it is the pattern speed of the spiral arms alone.

2.5 The Origin of the Pattern

Having measured the speed of the H I pattern in NGC 2915, we now consider the origin of the pattern. Is the pattern a phenomenon of the disk itself, or is it driven by other mechanisms?

2.5.1 Gravitational Interactions

Tidal triggering is a potentially important way to form bars, especially in dense environments. In the case of parabolic prograde planar encounters, Noguchi (1987) found that self-consistent disks (with a static halo) develop strong spiral structures over their entire length, with a bar-like pattern in their inner regions. Gerin, Combes, & Athanassoula (1990) also showed that interaction with a companion accelerates bar formation. The sense of interaction (prograde or retrograde) affects the bar growth rate and shape, with lesser effects on the strength and pattern speed of the resulting bar. When a bar already exists, its strength and pattern speed can again be affected by an interaction.

It seems unlikely that such scenarios can explain the structure of the disk in NGC 2915. No evidence of interaction is seen in the H I data of MCBF96, and the only catalogued potential interaction partner for NGC 2915, within $5°$, is a low luminosity, low surface brightness object, SGC 0938.1-7623, at a radius of $42'$ (projected distance of 65 kpc at the distance of NGC 2915). This object does not have a catalogued optical or H I velocity so, although there are no indications that NGC 2915 is interacting, we cannot definitively exclude this possibility.

2.5.2 Swing Amplification

Swing amplification (Toomre 1981) can generate spiral arms in a disk as transient tidal features. Although Toomre (1981) considered a stellar disk, his treatment should equally apply to gaseous disks. Swing amplification is a local cooperative effect: shear, epicyclic motions, and self-gravity all contribute to support the spiral pattern, originally excited by a small disturbance. The epicyclic motions resonate with the shear flow as the spiral pattern wraps, and the spiral arms are sustained. The self-gravity of the arms leads to a gravitational instability (Goldreich & Lynden-Bell 1965). These effects can be summarised (somewhat simplified by neglecting the shear) in Toomre's parameter X, given by

$$X = \frac{\lambda}{\lambda_{\rm crit}}, \tag{2.3}$$

where

$$\lambda_{\rm crit} = \frac{4\pi^2 {\rm G}\mu}{\kappa^2}, \tag{2.4}$$

μ is the surface density, and κ is the epicyclic frequency. Swing amplification is efficient for $X \lesssim 3$ (including the effects of shear and random motions; see, e.g., Fig. 7 of Toomre 1981). For an extended disk, we can write $\lambda = 2\pi r/m$, where m is the azimuthal wavenumber of the spiral pattern considered, and

$$X(r) = \frac{r\kappa(r)^2}{2\pi {\rm G} m\mu(r)} \tag{2.5}$$

(see Athanassoula, Bosma, & Papaioannou 1987).

Figure 2.5 shows $X(r)$ for NGC 2915 for two and four-armed spiral patterns. We use the surface density of the luminous matter only (gaseous and stellar), assuming that the dark matter is not responsive to the density perturbation created by the spiral pattern (Toomre 1981 considered a fixed halo). In Figure 2.5a, only the H I distribution from MCBF96 is included (see Table 2.2). It is clear from the figure that $X(r)$ is nowhere near a value of 3. In fact, even for $m = 4$, $X(r) \gtrsim 10$ for almost all radii. In Figure 2.5b, the stellar content is also included. To construct the surface density profile, we used the B surface brightness profile of MMC94 for $r < 125''$, and an extrapolation of their exponential fit to the outer parts of the disk for larger radii ($B(0)_c = 22.44$ mag arcsec^{-2} and $\alpha_B^{-1} = 25\farcs6$), with $M/L_B = 1.2\ M_\odot/L_{B,\odot}$ (as in the adopted mass model of MCBF96). The resulting surface brightness profile is tabulated in Table 2.2. Even with the stellar component, $X(r) \gtrsim 10$ for most radii. Small values of $X(r)$ are present in the inner regions only: $X(r) \leq 5$ for $r < 75''$ only. We note that those regions are within the rapidly rising portion of the rotation curve, where the bar resides and the shear is low, while swing amplification relies on shear to amplify the spiral pattern.

The work by Toomre (1981) refers to a flat rotation curve, $V_c(r) =$ constant, which is not exactly the case here. The amplification criterion $X \lesssim 3$ increases for higher shear rates (e.g. $X \lesssim 6$ for a Keplerian rotation curve, $V_c(r) \propto r^{-1/2}$) and decreases for smaller shear (e.g. $X \lesssim 1.5$ for $V_c(r) \propto r^{1/2}$; Toomre, private

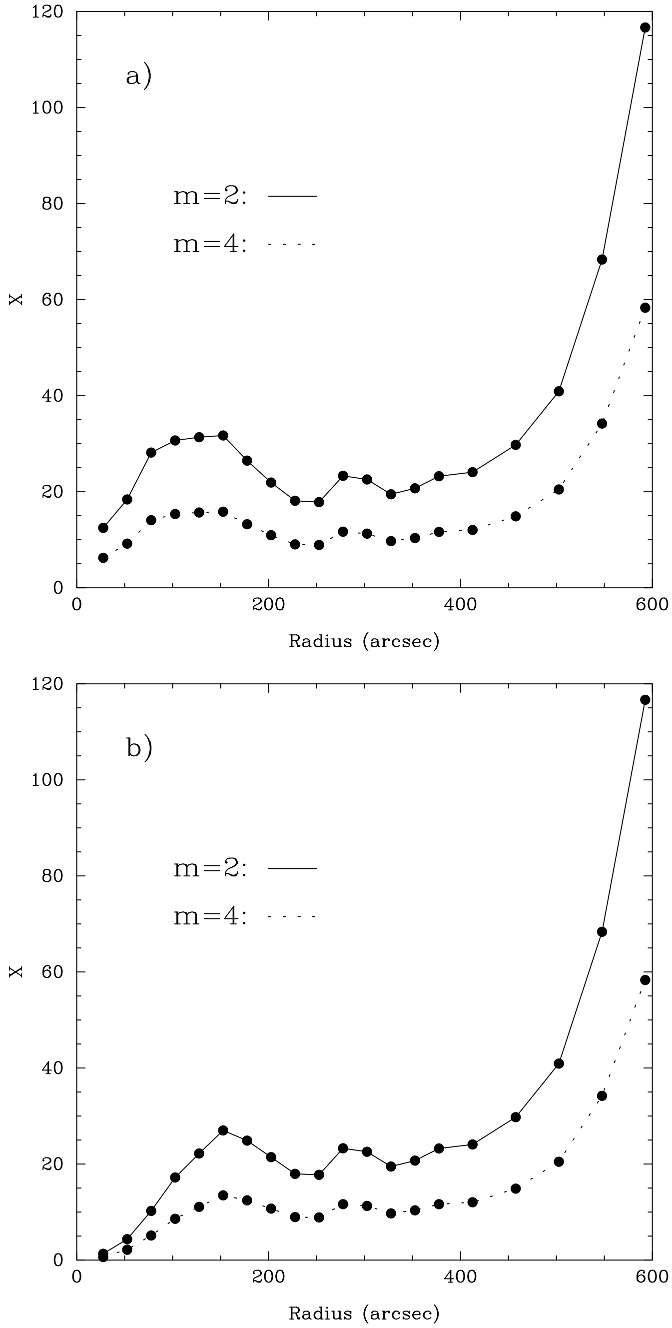

Figure 2.5: Calculated swing amplifier parameter $X(r)$ (eq. [2.5]) for two-armed ($m = 2$, full lines) and four-armed ($m = 4$, dotted lines) spiral patterns in NGC 2915. (a) shows $X(r)$ when only the H I distribution is taken into account, while in (b) both the H I and the stellar components are considered. $X \lesssim 3$ is required for swing amplification.

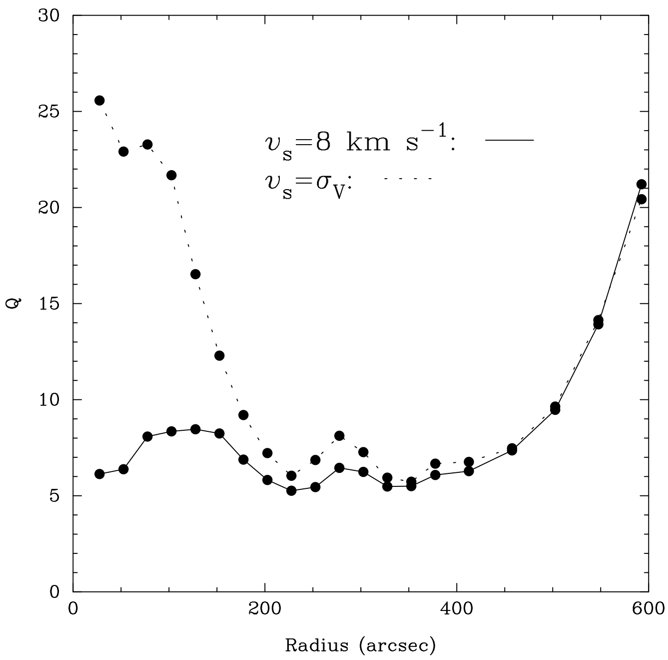

Figure 2.6: Calculated stability parameter $Q(r)$ (eq. [2.6]) in NGC 2915. The full line shows $Q(r)$ considering a fixed sound speed $v_s(r) = 8$ km s^{-1}, equal to the velocity dispersion in the outer parts of the H I disk. The dotted line assumes $v_s(r) = \sigma_v(r)$. $Q(r)$ scales directly with $v_s(r)$. $Q \gtrsim 2$ curbs swing amplification.

communication). So, if anything, the constraints on swing amplification are even stronger in the case of NGC 2915, especially in the inner parts.

Toomre's (1964) stability parameter Q also affects the efficiency of the swing amplifier mechanism. The stellar disk of NGC 2915 does not extend into the spiral pattern region, so we consider only the gaseous disk. Then,

$$Q(r) = \frac{v_s(r)\kappa(r)}{\pi \mathrm{G}\mu(r)}, \tag{2.6}$$

where v_s is the sound speed of the gas, taken here as the velocity dispersion. As Q increases, the maximum swing amplification factor decreases. For $V_c(r) =$ constant, $Q \gtrsim 2$ curbs most of the amplification (see, again, Fig. 7 of Toomre 1981). The criterion becomes $Q \gtrsim 3$ for $V_c(r) \propto r^{-1/2}$ and $Q \gtrsim 1.5$ for $V_c(r) \propto r^{1/2}$ (Toomre, private communication). Figure 2.6 shows $Q(r)$ for NGC 2915 using both a constant velocity dispersion, equal to the velocity dispersion in the outer parts of the H I disk, and the H I velocity dispersion profile of MCBF96, tabulated in Table 2.2. We see that $Q(r) \gtrsim 5$ everywhere, so the amplification factor would be small. In particular, $Q(r)$ is high in the inner regions. The sound speed would have to be less than 2–3 km s^{-1} to make $Q(r) < 2$ over a significant range of radii. Even then, X would still be too high for the swing amplifier to work efficiently.

Given the behaviour of $X(r)$ and $Q(r)$, and if the analogy between Toomre's

(1981) stellar treatment and our gaseous treatment is at least qualitatively valid[2], it seems clear that swing amplification cannot explain the spiral pattern seen in NGC 2915. Furthermore, given the very extended mass distribution of NGC 2915, it is unlikely that the observed spiral pattern results from an edge-mode, as discussed by Toomre (1981).

At this point, we conclude that the bar and spiral arms pattern in NGC 2915 is unlikely to be caused by gravitational interaction or swing amplification. We must therefore search for an alternative formation mechanism.

2.5.3 Bar-Driven Spiral Arms: Resonance Ring Formation

For a given rotation curve, the bar pattern speed is the most important parameter affecting the structure of barred spiral galaxies. It determines the presence and position of the resonances, and therefore the kind and extent of the orbit families present in the disk (see Sellwood & Wilkinson 1993). We can use the theory of resonance ring formation (Schwarz 1981, 1984; Byrd et al. 1994) to see if our pattern speed measurement is consistent with the location of the (pseudo-)rings seen in NGC 2915, and therefore determine whether the spiral arms could be driven by the bar.

Using the MCBF96 circular velocity curve, we can calculate the angular frequency of circular motion Ω and the associated Lindblad precession frequencies $\Omega + \kappa/2$, $\Omega - \kappa/2$, and $\Omega - \kappa/4$ (see Table 2.2). These are shown in Figure 2.7, along with the measured pattern speed and the position of various features in the disk of NGC 2915.

The first points in Figure 2.7 are affected by beam smoothing in the inner regions, but suggest the presence of an ILR ($\Omega_p = \Omega - \kappa/2$) at $r < 50''$. Nuclear rings are believed to be associated with ILRs, and usually form easily recognisable annuli of H II regions in the inner parts of galaxies. The shallower the rotation curve in the inner parts, the larger the nuclear ring formed (Byrd et al. 1994). However, no such ring is visible in the photometry of MMC94 or in the Fabry-Perot Hα images of Marlowe et al. (1995). The resolution of the H I data of MCBF96 is too low to resolve a ring of radius smaller than about $1'.5$.

The inner spiral arms seen in the total H I intensity map of NGC 2915 (Fig. 2.3) appear to form a pseudo-ring just outside the end of the bar, at a deprojected radius of $215 \pm 15''$. Inner rings are usually associated with the inner ultra-harmonic resonance ($\Omega_p = \Omega - \kappa/4$) which, in this case, occurs between about $190''$ and $340''$. This is just consistent with the position of the inner pseudo-ring.

[2]As mentioned by Toomre (1981) based on the work of Bardeen (1975) and Aoki, Noguchi, & Iye (1979), gaseous disks are probably more stable than stellar ones, which would strengthen our conclusions.

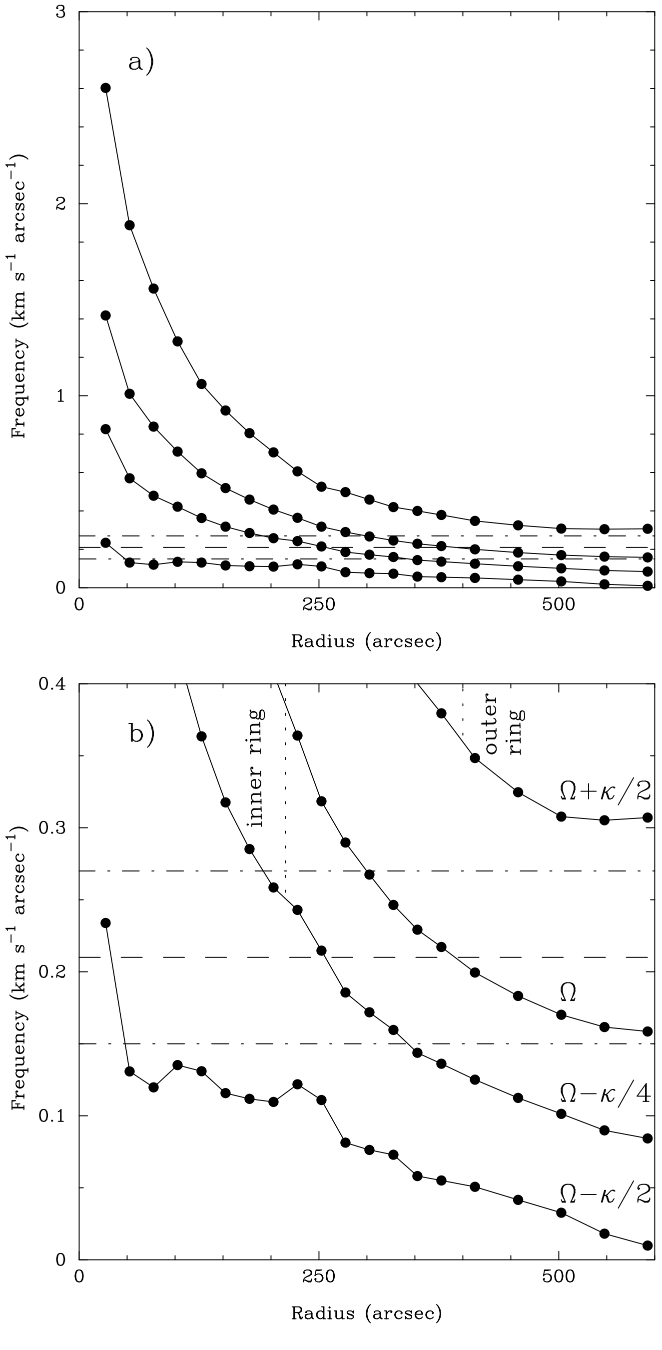

Figure 2.7: (a) Calculated Lindblad precession frequencies for NGC 2915 (solid lines). From top to bottom, they are, respectively, $\Omega + \kappa/2$, Ω, $\Omega - \kappa/4$, and $\Omega - \kappa/2$. The dashed line shows the adopted pattern speed Ω_p, while the dot-dashed lines show the range of values allowed by the uncertainty on Ω_p. (b) is simply an enlargement of (a), but in addition the position of various features in the disk of NGC 2915 are indicated (dotted vertical lines).

The outer spiral arms seen at the edge of the H I disk in Figure 2.3 form an outer pseudo-ring at $r = 400 \pm 15''$. Outer rings are normally associated with the outer Lindblad resonance ($\Omega_p = \Omega + \kappa/2$). However, the $\Omega + \kappa/2$ curve in Figure 2.7 does not intersect the range of measured values for Ω_p, which suggests that no outer Lindblad resonance is present in the disk of NGC 2915. Thus, no outer ring would be expected.

In summary, resonance ring theory has only limited success in explaining the position of the various (pseudo-)rings in NGC 2915 (nuclear, inner, and outer rings). It could be that the pattern in NGC 2915 is still evolving, and that the spiral arms are still in the process of forming rings. This seems unlikely, however, since no nuclear ring is detected, and the timescale for nuclear ring formation is very short (10^7 – 10^8 yr; Combes 1993). Stellar mass loss or gas infall can delay the formation of rings (Schwarz 1981), but these are improbable as most of the H I disk is devoid of stars and NGC 2915 is isolated.

Petrou & Papayannopoulos (1986) proposed a mechanism to terminate bars well within their corotation radius. This mechanism requires the presence of a 1:1 resonance ($\Omega_p = \Omega - \kappa$) in the bar, however, so it is clear from Figure 2.7 that it is not relevant in the case of NGC 2915.

We therefore conclude that the structures seen in the disk of NGC 2915 are probably not due to resonances and that the spiral pattern is not driven by the bar.

2.6 Dark Matter and the Structure of NGC 2915

The H I data of MCBF96 showed that NGC 2915 is dominated by dark matter, even in the central optical region of its disk. We now discuss the possible relations between the properties of this dominant dark matter distribution and the properties of the H I pattern.

2.6.1 Rotationally Supported Disk Dark Matter

Pfenniger, Combes, & Martinet (1994; see also Pfenniger & Combes 1994) propose that the dark matter required dynamically in disk galaxies is in the form of rotationally supported cold molecular gas. This idea is attractive for NGC 2915, as it would also provide the extra disk mass needed to explain the formation of the bar and spiral arms through gravitational instabilities in the disk. Unfortunately, observing such cold gas directly is difficult (for H_2, see Combes & Pfenniger 1997; for CO, see Lequeux & Allen 1993 and Wilson & Mauersberger 1994).

Figure 2.8a shows how much additional mass is required in the *disk* for the swing amplification mechanism to be efficient ($X = 3$ everywhere in the disk; see § 2.5.2). Similarly, Figure 2.8b shows how much additional disk matter is needed to lower Q to a value of 2 at all radii (the value required to make the disk gravitationally responsive). For comparison, we plot in Figure 2.8c the observed H I surface density (Table 2.2) and the projected surface density of the dark isothermal *sphere* used by MCBF96 to model the circular velocity curve (their model D), rescaled by a large constant factor (47.7).

The similarity between the H I and the dark matter surface density profiles seen in Figure 2.8c has been noticed before in other objects (e.g. Bosma 1978, 1981; Carignan & Beaulieu 1989; Broeils 1992) and has been interpreted as possible evidence that the H I and the dark matter are somehow associated. Here, we see in addition a qualitative similarity between the observed H I surface density profile and the surface density profile of the additional disk matter required to make $Q(r) = 2$ (Fig. 2.8b). It is tempting to regard this as further evidence that the dark matter is distributed in a disk and follows relatively closely the distribution of the neutral hydrogen. However, the increase in disk surface density required to make the swing amplifier work efficiently ($X = 3$ over most of the disk; Fig. 2.8a) would lower Q even more, and would make the disk unstable to axisymmetric modes. Figure 2.9 shows the ratio of the surface density obtained by imposing $X(r) = 3$ to Kennicutt's (1989) critical surface density for star formation in disks. This ratio is well above unity for the entire disk, so we would expect to see evidence for active star formation in the outer H I disk if the swing amplifier was working, which is not observed. It is therefore unlikely that dark matter distributed in a disk can account for all the properties of the H I disk in NGC 2915.

Nevertheless, it would be interesting to see if this type of argument, based on Toomre's (1964) parameter Q and the presence of a spiral pattern, could be used in other spiral galaxies to argue for the presence of a substantial amount of disk dark matter (see Quillen & Sarajedini 1998 for a similar application to intermediate-redshift galaxies).

2.6.2 Slowly Rotating Triaxial Dark Halos

Simulations of hierarchical structure formation in cold dark matter (CDM) universes predict that the dark halos around galaxies are triaxial in the mean, with some tendency to prolate shapes (Frenk et al. 1988; Dubinski & Carlberg 1991; Warren et al. 1992). The triaxiality and oblateness are slightly stronger in the outer parts but are almost independent of the halo mass and of the ratio V_r/σ_v (rotational velocity to velocity dispersion), indicating that the halos are supported by anisotropic velocity dispersions. The total angular momentum vector is nevertheless preferentially aligned with the minor axis of the mass distribution at all radii. When dissipation is included, the halos become more oblate while the

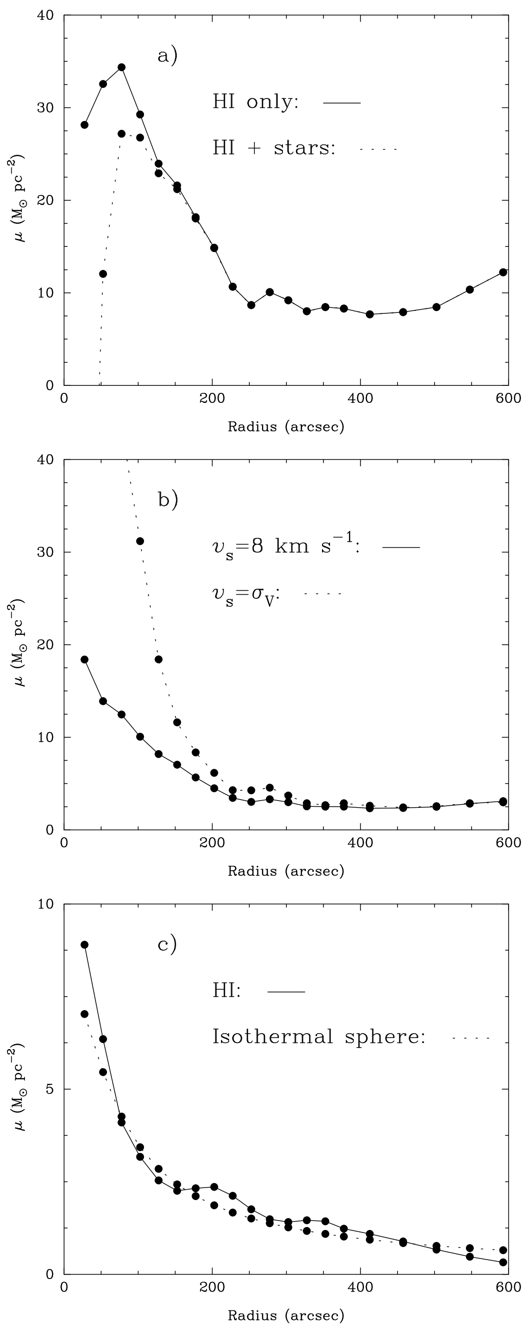

Figure 2.8: (a) Calculated disk dark matter surface density required to make the swing amplifier parameter $X(r) = 3$ (eq. [2.5]) for a two-armed ($m = 2$) spiral pattern in NGC 2915. The full line shows μ_{DM} when only the H I distribution is taken into account, while for the dotted line both the H I and the stellar component are considered. (b) Calculated disk dark matter surface density required to make the stability parameter $Q(r) = 2$ (eq. [2.6]). The full line shows μ_{DM} considering a fixed sound speed $v_s(r) = 8$ km s^{-1}, while the dotted line assumes $v_s(r) = \sigma_v(r)$. $Q(r)$ scales directly with $v_s(r)$. (c) The full line shows $\mu_{\rm HI}$, the observed disk surface density of H I (Table 2.2), while the dotted line shows μ_{DM}, the projected dark matter surface density of the dark isothermal sphere used by MCBF96 to model the rotation curve (their model D).

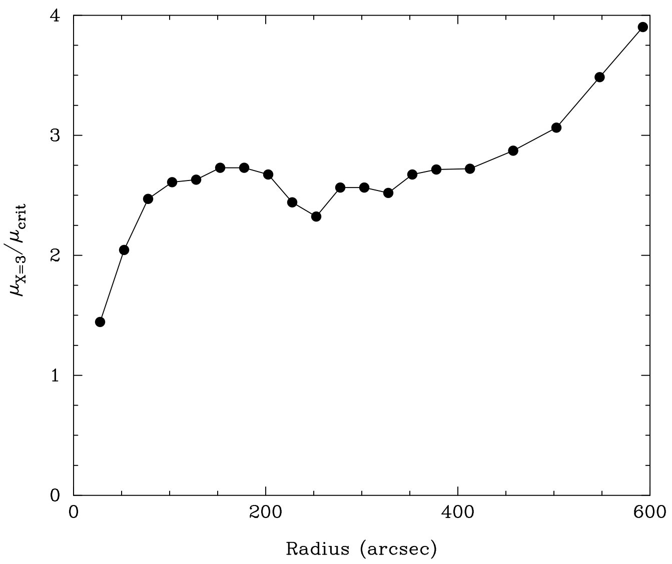

Figure 2.9: Calculated ratio of the total surface density required to make the swing amplifier parameter $X(r) = 3$ (eq. [2.5] with $m = 2$) to the critical surface density required for star formation in galactic disks (Kennicutt 1989) in NGC 2915.

flattening is unchanged (Dubinski 1994).

Observationally, the constraints on the shape of galactic halos remain weak. Polar-ring galaxies (e.g. Sackett et al. 1994) and the flaring (e.g. Olling 1995) and warping (e.g. Sparke 1984a) of the outer H I disk of spirals are usually used to constrain the three-dimensional structure of halos. Such studies often indicate flattened and sometimes triaxial dark halos (see also Becquaert & Combes 1997; Olling 1996), but are as yet inconclusive.

We now consider the possibility that the dark halo of NGC 2915 is triaxial, with its figure rotating slowly about the rotation axis of the H I disk, and that the H I bar and spiral arms in NGC 2915 are due to the forcing of the H I disk by this massive, extended, and rotating triaxial halo. The halo would then act much like a very massive, slowly rotating bar. This would readily explain why there is a unique pattern speed for the bar and spiral arms and why the bar ends so far from corotation (see § 2.4). The situation which we are proposing is similar to that of rotating weak oval distortions in disks, which are able to maintain an open spiral pattern to large radii (see, e.g., Hunter et al. 1988). This is in contrast to a more conventional bar, where the quadrupole term decreases too rapidly outside corotation (where the bar ends) to maintain an extended spiral structure.

The straight line of nodes of the warp in NGC 2915 (MCBF96) supports the suggestion of a triaxial halo. Displacements between the angular momentum vectors of the inner and outer regions of disks arise naturally in CDM models because of tidal torques. In an axisymmetric but flattened potential, the line of nodes would wrap quickly, but in a triaxial potential, the principal axes of the halo provide natural directions with which the warp can align (see Binney 1992 for a review of warps). Furthermore, an annulus of orbits circulating around the short axis of a triaxial halo becomes vertically unstable if the figure rotates, providing a natural way to excite a warp, although this may happen too far in the disk (outside corotation for prograde orbits) to be of interest here (Binney 1978, 1981; see also Sparke 1984b).

While the studies mentioned above (Frenk et al. 1988; Dubinski & Carlberg 1991; Warren et al. 1992; Dubinski 1994) have shown that the dark halos in CDM cosmological simulations can be strongly triaxial and have well-defined angular momentum properties (with flat rotation curves extending up to the core), only their instantaneous shapes and the rotational motions within the figures (streaming) have been studied. As far as we are aware, there has been no systematic study of the *figure* rotation of these triaxial halos.

Prompted by this work, Pfitzner began a study, to be published elsewhere, of the figure rotation of halos in a set of large CDM structure formation simulations. The shape distribution of the halos varies systematically with both radius and mass, but for our current purposes it suffices to say that many halos are significantly triaxial, as in other studies. Following the orientation of each halo over time, Pfitzner finds that a subset of the triaxial halos exhibits steady figure rotation about the minor axis. The statistics of how many halos in the simulations have figure rotation is confused by numerical resolution issues, but the fraction is clearly significant. To verify that these results are not due to transient phenomena, one of the rotating halo candidates was extracted and evolved in isolation. The halo displayed no systematic change of density or shape over the simulation time of 5 Gyr. Figure 2.10 shows that the figure of this triaxial halo rotates as a solid body with constant pattern speed. Hence we conclude that at least some halos in these CDM simulations do exhibit genuine steady slow figure rotation over a Hubble time. These simulations are not yet directly applicable to the example of NGC 2915, because the halos are much more massive than that of NGC 2915. They do, however, suggest that an underlying triaxial dark halo with figure rotation may make an important contribution to the dynamics of the outer H I disk of some galaxies. If this is correct, it also offers another way to measure the shape of (triaxial) dark halos from detailed H I velocity field, using methods similar to those of Franx, van Gorkom, & de Zeeuw (1994).

The slow pattern speeds found in the present study and in the above simulations are interesting in the context of recent work by Miwa & Noguchi (1998). They made N-body simulations of barred galaxies in which the bars arose (1) spontaneously in marginally stable disks, and (2) through the effect of a tidal interaction in more stable disks. The pattern speeds of the spontaneous bars are fast, with corotation near the ends of the bars, as expected in self-consistent sys-

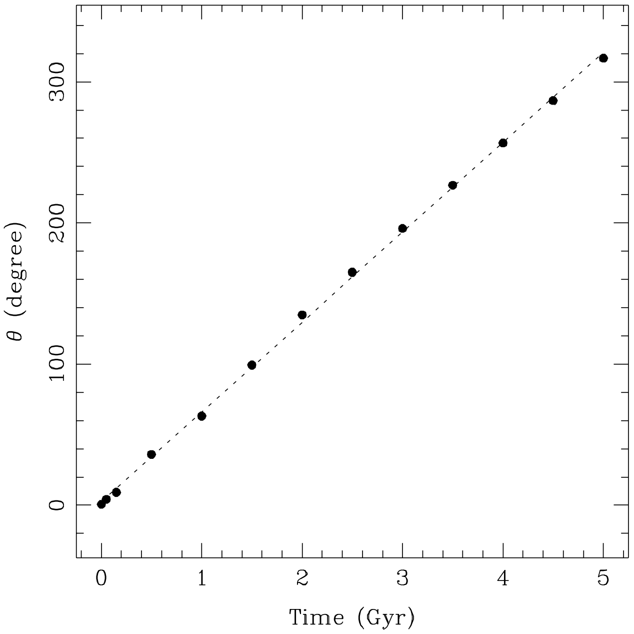

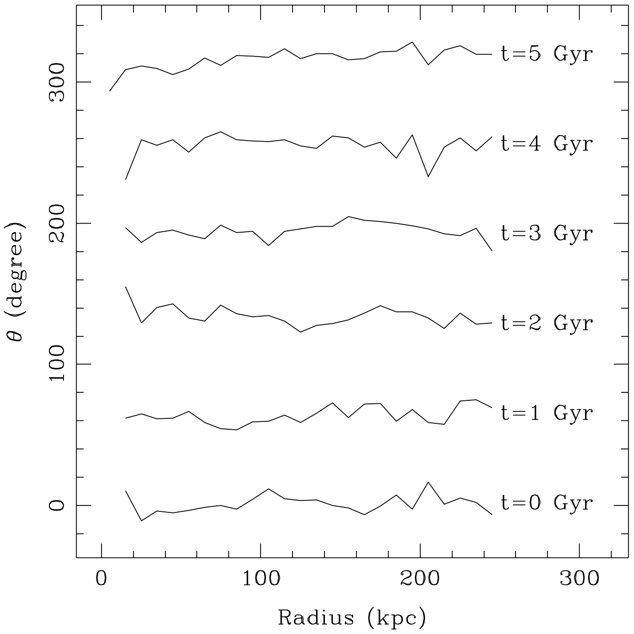

Figure 2.10: (a) Orientation of the major axis of a dark halo formed in a CDM simulation as a function of time. The angle θ is measured in a fixed plane perpendicular to the minor axis (the rotation axis). Filled circles show the mean orientation of the halo as a function of time, and the dotted line is a linear fit to the data, showing that the halo pattern speed is constant. (b) Orientation of the major axis of the same halo as a function of radius (in isodensity-defined shells) for selected times, showing that the halo rotates as a solid-body.

tems. In the tidally induced bars, however, the pattern speeds are generally much slower, and the bars appear to be limited by the ILR, rather than by corotation. In particular, any relatively large tidal disturbance leads to a slow pattern speed, independent of the original properties of the disk. These results may be relevant to the pattern speeds of the triaxial dark halos formed in CDM simulations, in which the triaxiality results at least partially from tidal effects during the aggregation process.

2.7 Conclusions

We applied the method of Tremaine & Weinberg (1984) to measure the pattern speed in the galaxy NGC 2915, using neutral hydrogen as the tracer and radio synthesis data. NGC 2915 is a BCD galaxy with a very extended H I disk showing an open barred spiral morphology. It is also completely dominated by dark matter. Our measurements yield a pattern speed of 8.0 ± 2.4 km s^{-1} kpc^{-1} for $D =$ 5.3 Mpc. This pattern speed is inconsistent with the generic property of self-consistent barred disks, that corotation occurs just outside the end of the bar. Our adopted bar length puts corotation at more than 1.7 bar radii. We considered the possibility that the bar and spiral arms have different pattern speeds and demonstrated that this is unlikely.

NGC 2915 is isolated, so gravitational interactions are unlikely to explain the strong bar and spiral pattern observed in the H I disk. Because the surface density in the disk is so low, Toomre's (1981) swing amplification mechanism is also unable to explain the origin of the pattern. Furthermore, resonance ring theory fails to predict successfully the position of the pseudo-rings seen in the disk of NGC 2915, indicating that the spiral arms are not driven by the bar itself.

This lead us to consider two scenarios, involving different dark matter distributions, to explain the structure and dynamics of the H I disk in NGC 2915. Firstly, we considered dark matter in near-circular motion, distributed in a disk, and following closely the distribution of H I, as suggested by the similarity of the dark matter and H I surface density profiles. This does not appear to work: if the dark matter disk is dense enough for the swing amplifier to function efficiently, then the disk becomes unstable to axisymmetric disturbances and we would expect to see evidence for star formation, which is not observed. Secondly, we considered the effects of dark matter distributed in a massive pressure-supported halo with extended triaxiality, like the halos seen in CDM cosmological simulations. In addition, we required the halo to have a slow figure rotation. Such figure rotation is seen in the preliminary analysis of a set of CDM simulations, which show triaxial halos with figure rotation constant over many Gyr. This kind of model can explain the structure in the disk of NGC 2915 through the torques exerted by the slowly rotating triaxial figure of the dark halo.

The H I structure in NGC 2915 is visible because the H I synthesis observations were made at a relatively high spatial resolution (beam FWHM of about 650 pc for the uniformly weighted data and about 1150 pc for the naturally weighted data). As far as we are aware, NGC 2915 is the only galaxy showing such structure in an extended H I disk. If our suggestions are correct, it would be very desirable to have H I observations of similar spatial resolution for other nearby galaxies with extended H I disks, as those observations could provide similar probes of the dynamics of their dark halos. Our argument on figure rotation also relies heavily on the theory of the forcing of structures by oval distortions in disk galaxies, in a situation which is not precisely analogous to that in NGC 2915. Hydrodynamical simulations of gas disks in the potentials of triaxial halos with figure rotation would thus be very welcome.

References

Aoki, S., Noguchi, M., & Iye, M. 1979, PASJ, 31, 737

Athanassoula, E. 1992a, MNRAS, 259, 328

———. 1992b, MNRAS, 259, 345

Athanassoula, E., Bosma, A., & Papaioannou, S. 1987, A&A, 179, 23

Athanassoula, E., & Sellwood, J. A. 1986, MNRAS, 221, 213

Bardeen, J. M. 1975, in Dynamics of Stellar Systems, ed. A. Hayli (Reidel), 297

Becquaert, J.-F., & Combes, F. 1997, A&A, 325, 41

Begeman, K. G. 1989, A&A, 223, 47

Binney, J. J. 1978, MNRAS, 183, 779

———. 1981, MNRAS, 196, 455

———. 1992, ARA&A, 30, 51

Bosma, A. 1978, Ph.D. Thesis, University of Groningen

———. 1981, AJ, 86, 1971

Broeils, A. H. 1992, A&A, 256, 19

Byrd, G., Rautiainen, P., Salo, H., Buta, R., & Crocker, D. A. 1994, AJ, 108, 476

Carignan, C., & Beaulieu, S. 1989, ApJ, 347, 760

Carignan, C., & Freeman, K. C. 1985, ApJ, 294, 494

Carr, B. 1994, ARA&A, 32, 531

Combes, F. 1993, in N-Body Problems and Gravitational Dynamics, ed. F. Combes & E. Athanassoula (Paris: Observatoire de Paris), 137

Combes, F., & Pfenniger, D. 1997, A&A, 327, 453

Combes, F., & Sanders, R. H. 1981, A&A, 96, 164

Contopoulos, G. 1980, A&A, 81, 198

Contopoulos, G., & Grosbøl, P. 1989, A&A Rev., 1, 261

Debattista, V. P., & Sellwood, J. A. 1998, ApJ, 493, L5

Dubinski, J. 1994, ApJ, 431, 617

Dubinski, J., & Carlberg, R. G. 1991, ApJ, 378, 496

Franx, M., van Gorkom, J. H., & de Zeeuw, T. 1994, ApJ, 436, 642

Frenk, C. S., White, S. D. M., Davis, M., & Efstathiou, G. 1988, ApJ, 327, 507

Gerin, M., Combes, F., & Athanassoula, E. 1990, A&A, 230, 37

Goldreich, P., & Lynden-Bell, D. 1965, MNRAS, 130, 125

Hunter, J. H., Ball, R., Huntley, J. M., England, M. N., & Gottesman, S. T. 1988, ApJ, 324, 721

Kalnajs, A. J. 1971, ApJ, 166, 275

———. 1977, ApJ, 212, 637

———. 1996, in Barred Galaxies and Circumnuclear Activity, ed. Aa. Sandqvist & P. O. Lindblad (Berlin: Springer), 165

Kennicutt, R. C. Jr. 1989, ApJ, 344, 685

Kent, S. M. 1987, AJ, 93, 1062

Kormendy, J. 1984, ApJ, 286, 132

Kuijken, K., & Merrifield, M. R. 1996, in Barred Galaxies, ed. R. Buta, D. A. Crocker, & B. G. Elmegreen (San Francisco:ASP), 215

Lequeux, J., & Allen, R. J. 1993, A&A, 280, L23

Lindblad, P. A. B., & Kristen, H. 1996, A&A, 313, 733

Lindblad, P. A. B., Lindblad, P. O., & Athanassoula, E. 1996, A&A, 313, 65

Marlowe, A. T., Heckman, T. M., Wyse, R. F. G., & Schommer, R. 1995, ApJ, 438, 563

Merrifield, M. R., & Kuijken K. 1995, MNRAS, 274, 933

Meurer, G. R., Carignan, C., Beaulieu, S. F., & Freeman, K. C. 1996, AJ, 111, 1551 (MCBF96)

Meurer, G. R., Mackie, G., & Carignan, C. 1994, AJ, 107, 2021 (MMC94)

Miwa, T., & Noguchi, M. 1998, ApJ, 499, 149

Noguchi, M. 1987, MNRAS, 228, 635

Olling, R. P. 1995, AJ, 110, 591

———. 1996, AJ, 112, 481

Ousley, D., Byrd, G., & Dalla Piazza C. 1997, BAAS, 29, 1333

Petrou, M., & Papayannopoulos, T. 1986, MNRAS, 219, 157

Pfenniger, D., & Combes, F. 1994, A&A, 285, 94

Pfenniger, D., Combes, F., & Martinet, L. 1994, A&A, 285, 79

Quillen, A. C., & Sarajedini, V. L. 1998, AJ, 115, 1412

Raha, N., Sellwood, J. A., James, R. A., & Kahn, F. D. 1991, Nature, 352, 411

Ryder, S. D., Buta, R. J., Toledo, H., Shukla, H., Staveley-Smith, L., & Walsh, W. 1996, ApJ, 460, 665

Sackett, P. D., Rix, H.-W., Jarvis, B. J., & Freeman, K. C. 1994, ApJ, 436, 629

Sancisi, R., Allen, R. J., & Sullivan, W. T. 1979, A&A, 78, 217

Schmidt, K.-H., & Boller, T. 1992, ANac, 313, 189

Schwarz, M. P. 1981, ApJ, 247, 77

———. 1984, MNRAS, 209, 93

Sellwood, J. A. 1980, A&A, 89, 296

———. 1981, A&A, 99, 362

Sellwood, J. A., & Sparke, L. S. 1988, MNRAS, 231, 25

Sellwood, J. A., & Wilkinson, A. 1993, Re. Prog. Phys., 56, 173

Sparke, L. S. 1984a, ApJ, 280, 117

———. 1984b, MNRAS, 211, 911

Sparke, L. S., & Sellwood, J. A. 1987, MNRAS, 225, 653

Sygnet, J. F., Tagger, M., Athanassoula, E., & Pellat, R. 1988, MNRAS, 232, 733

Tagger, M., Sygnet, J. F., Athanassoula, E., & Pellat, R. 1987, ApJ, 318, L43

Teuben, P. J., & Sanders, R. H. 1985, MNRAS, 212, 257

Toomre, A. 1964, ApJ, 139, 1217

———. 1981, in Structure and Evolution of Normal Galaxies, ed. S. M. Fall & D. Lynden-Bell (Cambridge: Cambridge University Press), 111

Tremaine, S., & Weinberg, M. D. 1984, ApJ, 282, L5

Trimble, V. 1987, ARA&A, 25, 425

Warren, M. S., Quinn, P. J., Salmon, J. K., & Zurek, W. H. 1992, ApJ, 399, 405

Weinberg, M. D. 1985, MNRAS, 213, 451

Wilson, T. L., & Mauersberger, R. 1994, A&A, 282, L41